

2009 ASME Human Powered Vehicle Competition

Drexel University
Philadelphia PA

DESIGN REPORT

Olin College Human Powered Vehicle *Helios*

Franklin W. Olin College of Engineering



Co-Captains: Pamela Darvirris and David Stamp

Casey Canfield, Elsa Culler, Pamela Darvirris, Giulia Fanti, Jacob Felser, David Gardner, Carl Herrmann, Jacob Izraelevitz, Ariel Leigh, Aaron Marcuze-Kubitza, Alex Niswander, John Rosenwinkel, Travis Schuh, David Stamp, Boris Taratutin, Gray Thomas, Lorraine Weis, Steven Zhang

March 20, 2009

CONTENTS

| | | |
|-----|------------------------------------|----|
| 1 | Abstract..... | 3 |
| 2 | Design and Innovation | 3 |
| 2.1 | Frame | 4 |
| 2.2 | Drivetrain | 5 |
| 2.3 | Steering Design | 7 |
| 2.4 | Seat | 8 |
| 2.5 | Roll Bar Design | 10 |
| 2.6 | Fairing Design..... | 10 |
| 3 | Analysis | 12 |
| 3.1 | Frame Analysis | 13 |
| 3.2 | Fairing Analysis..... | 15 |
| 3.3 | Roll Bar Analysis | 17 |
| 3.4 | Drivetrain Analysis | 21 |
| 3.5 | Vehicle Cost Analysis..... | 22 |
| 4 | Testing..... | 23 |
| 4.1 | Drivetrain Efficiency | 23 |
| 4.2 | Speed and Stability Testing | 25 |
| 4.3 | Fairing Construction Testing | 26 |
| 4.4 | Roll Bar Testing..... | 27 |
| 5 | Safety | 28 |
| 6 | Bibliography | 29 |

1 ABSTRACT

The Olin College Human Powered Vehicle Team returns for its third year at the ASME HPV competition with *Helios*. Our main goals this year were to improve our bicycle's efficiency, maneuverability, and ridability. We were able to finish a prototype early in order to give our riders an idea of the final vehicle handling and provide feedback. As a result of this prototype, we discovered improvements that could be included in our final vehicle. Since the construction process of the final vehicle was similar to the prototype, we were able to finish early, giving riders ample practice with the vehicle. For example, we are now comfortable enough to ride our vehicle several miles to the grocery store.

Similar to last year's *Vega*, *Helios* is a fully-faired recumbent bicycle, constructed in Olin College's machining facilities. However, our current vehicle design includes substantial changes from our previous iterations:

1. Unlike any of our previous vehicles, *Helios* is rear wheel drive. We expect this change to improve our maneuverability, stability, and rider comfort, as well as drastically improve our chain alignment and reliability.
2. Our frontal area is larger than last year's *Vega*, but we account for this loss in aerodynamics with a full composite fairing. This full fairing is constructed with our new and highly innovative manufacturing process which will allow us to fabricate composites on a larger scale.
3. Unlike *Vega*'s seat attachment method, our seat is simultaneously adjustable and rotationally constrained. We expect this will make changing riders significantly easier during the endurance event.

We also substantially increased the number and variety of performance tests, again due to the early completion of the *Helios* and the prototype. In addition to the standard FEA analysis on stress and aerodynamics, we developed simple methods to determine the drivetrain efficiency and maneuverability of the vehicles. These tests directly informed our design decisions, allowing us to confidently produce an optimized vehicle design.

One of the new methods of pre-testing that we incorporated this year was miniature fairing prototyping. We built small models of our cardboard honeycomb out of paper and put them together. From this we were able to modify the connections between the pieces as well as notice any deficient areas in the design.

We hope to be more competitive this year than in previous years. Increased reliability of our vehicle will be a large factor in determining our success.

2 DESIGN AND INNOVATION

Now in our third year of competition, we have considerable experience to guide our design and decision-making process. Reflection on our performance in years past highlighted several weaknesses in our vehicle design. Our failure to produce a full composite fairing last year contributed to poor vehicle performance and low team morale throughout the competition. We decided that a full fairing must be at the top of our list to accomplish this year. The other major problem cited with previous vehicles was reliability. Our first year of competition we led the first third of the endurance race until failure of components and poor chain retention gave other teams an advantage, and similar problems plagued us last year as well. In response we have made reliability the guiding focus of our design process this year. Based on previous experience, we believe that concentrating our efforts on reliability in every aspect of our design will be the best use of our limited manpower, producing a design that will give us the best chance of success at competition and a solid foundation from which to refine future designs.

We began this year's design process with a period of background research and creative ideation. Out of this came a number of innovative ideas, the most promising of which were incorporated into a prototype vehicle for evaluation. The design of the prototype was intended to give new team members experience with our design process and vehicle construction techniques, and to enable side by side comparison of new features such as the

drivetrain with previous vehicles. Following construction and testing of the prototype, we began rigorous design of the year's competition vehicle.

2.1 FRAME

For our initial prototype, we considered a wide range of concepts, from a low-riding frame very similar to past designs to an unusual overhead frame from which the rider would have been suspended. We eventually selected a frame with higher ground clearance and a more upright rider position compared to the *Aurora* (2006-07) and *Vega* (2007-08) in an attempt to correct stability and handling problems we experienced in the past. The overhead frame, while interesting, would have created a whole host of new issues to deal with; the design is better suited to a project outside the time constraints of the competition when time is available for experimentation. Other frame concepts were similarly not chosen for this prototype, as we decided to use the short time available for the prototype to directly address issues we identified with our vehicles in the past.

We constructed and tested our prototype vehicle (see Section 3.2), evaluating its performance side by side with the *Vega*. We immediately began using the experience and knowledge gained from this new vehicle to inform our design decisions for *Helios*. From our perspective we saw several options in terms of frame geometry in the design space defined by the conventional, forward-facing, recumbent rider position. This rider position is by far the most common design in use today for good reason, as it optimizes rider comfort and ease of riding. Having investigated published HPV designs and constructed several different designs ourselves, we were faced with several design possibilities, including a small, low-riding design similar to our previous vehicles, a taller, more stable vehicle similar to our prototype design, and an overhead design and other concepts from initial prototype frame ideation.

We evaluated our different fairing options on several comparative metrics, assigning each option a numerical rating according to how well it fulfilled the metric. This method weights each criterion equally and is somewhat arbitrary; the results should be taken lightly but can be used to guide the design process. Table 1 shows a comparison of the different options we considered: a low rider like last year's *Vega*, our prototype, an overhead frame (in which rider is suspended below the frame), and a conventional bicycle (as a control). The criteria we used for comparison were: aerodynamics of fairing (frontal area), ergonomics and rider comfort, stability, team experience with frame type, and innovation of frame geometry.

| Criteria | <i>Vega</i> | Prototype | Overhead | Standard Bicycle |
|---------------|-------------|-----------|-----------|------------------|
| Aerodynamics | 4 | 3 | 2 | 1 |
| Ergonomics | 2 | 3 | 1 | 4 |
| Stability | 1 | 3 | 2 | 4 |
| Experience | 4 | 3 | 1 | 2 |
| Innovation | 2 | 3 | 4 | 1 |
| TOTALS | 13 | 15 | 10 | 12 |

TABLE 1: COMPARISON OF DIFFERENT FRAME GEOMETRY OPTIONS, WITH RELATIVE SCORES FOR EACH CRITERION.

While the *Vega* had excellent aerodynamics and, after two years of similar vehicles, we have considerable experience with low riders, it suffers from poor stability, limited rider comfort, and would not be an innovative new concept for our team. Our control, a conventional bicycle, is stable and comfortable for the rider, but is not innovative or aerodynamic. Although the overhead frame geometry is our most innovative concept, we foresee problems resulting from our lack of experience, particularly with regards to ergonomics. This left our prototype geometry; it will have a larger frontal area than the low riding *Vega* but improves comfort, stability, and, being a new concept for our team this year, forces us to innovate and expand our experience to new vehicle design.

Another crucial decision to be made for the design of our frame was the material. All of our past vehicles have used thin-walled steel tube, but other materials would be somewhat lighter or provide different structural

characteristics. Standard 6061-T6 aluminum tubes, for example, provide the same tensile strength as our 4130 steel tubes with about half the weight. We presently lack machining capability to work with titanium, but it is widely used in the bicycle industry. Another option we discovered with some research was the use of bamboo as a frame material (Wired.com, 2008). Bamboo has the strength and weight properties prized by bicycle makers; the only difficulty comes in attaching bamboo pieces to one another and to the metal components of the drivetrain. Regardless, we considered bamboo an interesting and viable alternative to metals, and certainly a step towards a more environmentally friendly human powered vehicle (American Bamboo Society, 2008).

| Criteria | Steel | Aluminum | Bamboo |
|---------------|-----------|----------|----------|
| Experience | 3 | 2 | 1 |
| Cost | 2 | 1 | 3 |
| Attachment | 3 | 2 | 1 |
| Fatigue | 3 | 2 | 1 |
| Weight | 1 | 2 | 3 |
| TOTALS | 12 | 9 | 9 |

TABLE 2: COMPARISON OF DIFFERENT FRAME MATERIALS.

Table 2 shows a comparison of the different prospective vehicle frame materials. Aluminum is lighter than an equivalent steel frame, but similar in cost. Unfortunately, we have not worked with it before and lack experience welding thin aluminum tubes. Aluminum also has more problems with fatigue failure than steel (Smith, 1985); we have already had fatigue problems with our vehicles and believe the choice of aluminum would exacerbate these problems. While bamboo is possibly our lightest and most inexpensive material option, we were unable to find documentation of its material properties so can't say for certain how its strength and resilience compares to the metals. We also have no experience working with it and have serious concerns integrating bamboo with conventional bicycle components like bottom brackets and steering tubes. This leaves us again with steel, not the lightest material, but available at reasonable cost and easily welded by inexperienced welders. However, bamboo shows promise and we were very impressed by the bamboo bicycles that turned up in our research; we intend to investigate this material further, perhaps conducting our own material property tests to characterize its structural properties.

2.2 DRIVETRAIN

Designing the drivetrain for *Helios*, we focused on speed, efficiency, and our overarching goal of reliability. For our speed goal, we decided being capable of achieving at least the maximum speed record for the HPVC, about 45mph, would provide a solid design point. Additionally, the chain disengaged often last year, as the front wheel intersected it during turns. Rear wheel drive solves this problem because the chain can be routed around the front wheel. However, we were not sure whether efficiency losses would be significant using this new type of drive. In order to meet our goal of a reliable vehicle and decide the best drivetrain method, we explored the feasibility of rear wheel drive.

On the last rear wheel drive vehicle built by our team, a single chain connected the front crankset to the rear cassette with chain routing accomplished by a number of rollers. These rollers were inefficient and unreliable; on more recent front wheel drive vehicles, chain routing was done using separate chain loops connected at interchanges. Using interchanges eliminated the need to use rollers or idler sprockets and enabled additional gearing, if necessary, by using different sized sprockets at the interchange.

The frame geometry from our prototype lent itself to two interchanges, one at each bend in the frame. We decided it was possible to use just a single interchange on *Helios*. This would make the drivetrain slightly more efficient by eliminating unnecessary components and would simplify manufacturing. We discovered several problems with the prototype's drivetrain, learning that this design is sensitive to placement of components in

relation to the front wheel and fork. Without precise placement of the chain, interference can occur with the wheel, fork, brakes, and other components.



FIGURE 1: THE PROXIMITY OF THE CHAIN PATH TO THE BRAKES AND FRONT FORK NECESSITATES MOUNTING BRAKES BACKWARDS BECAUSE OF INTERFERENCE ISSUES.

The single interchange concept also minimizes points of failure for the drivetrain while avoiding the inefficiency associated with a single, long chain; extra sprockets and chains simply mean more locations for the chain to detach. Failure of the drivetrain due to chain failure has been a problem in the past and we sought to minimize or eliminate this mode by simplifying the drivetrain and designing for reliability.

To start, we successfully integrated rear wheel drive into our prototype. Although the system needed some changes, it appeared that the rear wheel drive system could be made into a high quality, reliable drivetrain for competition. Using knowledge gained from our prototype, we compared front versus rear wheel drive, evaluating criteria such as efficiency, level of experience, and reliability.

| Criteria | FWD | RWD |
|------------------|----------|----------|
| Experience | 1 | 1 |
| Weight | 1 | 0 |
| Size | 1 | 0 |
| Efficiency | 1 | 1 |
| Reliability | 0 | 1 |
| Limited Pedaling | 0 | 1 |
| TOTALS | 4 | 4 |

TABLE 3: DRIVETRAIN DECISION MATRIX.

Due primarily to the much longer chain path required of a rear wheel drive system, we gave the weight advantage to front wheel drive. Front wheel drive also has the advantage of being very compact, as it is contained entirely in the front of the vehicle and does not require chain routing around the rider to the rear wheel. Using rear wheel drive forces the bike to be higher off the ground in order to leave room for the chain to run underneath the bike. Chain twisting, such as that seen when turning with front wheel drive, impacts efficiency. However, in testing (see

Section 3.1) we found that front and rear wheel drive had similar efficiencies in all situations that the bike was to encounter.

Both drivetrain options received the same number of points in our subjective analysis. However, since our underlying design goal this year was reliability, we decided to implement the rear wheel drive despite its bulk. Using rear wheel drive also inherently made the vehicle easier to ride, as it raised the wheelbase and increased stability by raising center of mass.

In some of our preliminary background research, one of our team members ran across the “k-drive” concept for producing elliptical, or even linear, pedal paths instead of the traditional circular path. It is an interesting mechanical concept and certainly has its place when designers are space-constrained or under other limitations necessitating a limited pedal path. We took the idea under consideration for our vehicle, but as shown in Table 4, the additional design and manufacturing work created by “k-drive” concept more than outweighs its benefit in compactness. The “k-drive” is suited to reducing or changing the geometry of the volume swept out by pedaling, which could be useful in designing the fairing, and our research suggests the system’s efficiency might be similar to conventional cranksets. However, many of the components of the “k-drive” would need to be custom-built, as we know of no commercially available options, and the system’s complexity adds additional weight and points of failure, potentially hurting our reliability goals.

| CRITERIA | K-DRIVE | STANDARD |
|-------------------|----------|----------|
| Experience | 0 | 1 |
| Manufacturability | 0 | 1 |
| Robustness | 0 | 1 |
| Compactness | 1 | 0 |
| Efficiency | 1 | 1 |
| Weight | 0 | 1 |
| TOTALS | 2 | 5 |

TABLE 4: CRANK OPTIONS DECISION MATRIX.

2.3 STEERING DESIGN

On the *Helios* we are using a double-push rod for the steering, similar to what we have employed on previous vehicles. This system is reliable, easy to operate, and easy to manufacture. One of our design goals for the vehicle is to enable all members of our team to ride. Accomplishing this required adjustable steering such that our shorter riders are not jammed in the stomach by the double-push rod. We built extender bars off of the base steering that will accommodate every rider. As seen in the figure below, these are secured by a lock nut and can be adjusted easily when changing riders.



FIGURE 2: STEERING SYSTEM OF *HELIOS*, SHOWING DOUBLE PUSHROD SETUP WITH ADJUSTABLE LENGTH HANDLEBARS IN UPPER LEFT.

2.4 SEAT

We designed the seat based on our experiences with our previous seats. The objective of the seat is to provide a solid structure that supports the rider yet can be adjusted to accommodate riders of different heights. In past years, the seat had a tendency to rotate around the main frame tube if the adjustment mechanism was not tightened properly. In order to design for maximum usability, we focused on making an adjustment mechanism that slid smoothly and naturally maintained a vertical alignment. At the same time, we designed for manufacturing, discarding ideas that would have taken too much time or resources, such as a full composite seat.

Part of our design of the seat rested on the ability to eliminate extraneous or unnecessary degrees of freedom from movement. Of the three degrees of translational freedom, we wanted only one along the axis of the frame tube. Any up/down or side-to-side seat movement would create instabilities while riding the vehicle. Rotationally, we wanted all degrees of freedom to be eliminated, as they do not contribute anything to needed seat movement. In the past, we had rotational freedom around the frame tube, causing the seat to tilt, affecting center of balance and rideability. When considering designs for Helios we marked rotation as especially important.

As a starting point we brainstormed various designs, ignoring practicality and ease of manufacture. These solutions included attaching the seat to the roll bar, using a square frame tube for attachment, sliding only the back of the seat, and welding a tube to the underside of the frame tube for consistent sliding. Of these, we seriously considered the latter three.

The first of these ideas, using a square frame tube, achieved our goal of no rotation and appeared to be relatively easy to manufacture. However, the square tube would be harder to acquire as well as more expensive for same size tubes. Cost-wise it was much cheaper to go with a circular tube, as we already had some available. For our second idea, sliding only the back of the seat, we could not think of a way to conceptualize our idea into a feasible design. For these reasons we decided on our last proposition as our seat design.

Our chosen design solves the problem of rotation without requiring a complicated mechanism. We integrated the idea into our prototype, finding that it worked fairly well, only needing minor adjustments. For one, we found that the seat was harder to move than anticipated. This can be attributed to the lack of throw inherent to the quick

release holding our seat to the frame. Even when fully released the clamp significantly contacted the frame tube, making movement difficult. To address this issue we built additional iterations of the clamp with increased rigidity to reduce the throw necessary to clamp and release sufficiently. We fabricated two designs, a top-bottom hinge and a left-right hinge. After implementing both designs on the vehicle we found the left-right clamp best for the seat, as it was easier to use as well as slightly lighter.

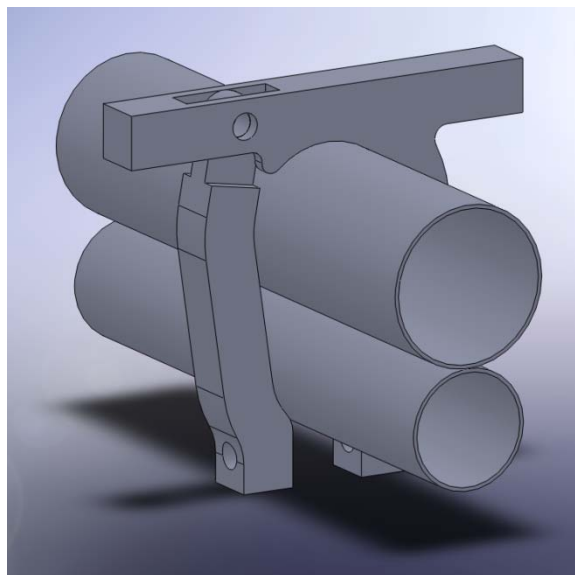


FIGURE 3: LEFT-RIGHT CLAMP CONCEPT SHOWN AROUND THE LARGE MAIN FRAME TUBE AND SMALLER SUPPORT TUBE.

Through building a prototype we found that although our clamp restrained the seat from rotating, it was harder to move the seat than we anticipated. This was because the quick release we used for the clamp did not have much throw and even when it was fully released there was still significant contact between the seat and the clamp, making it hard to slide the seat. To address this issue we decided to make additional iterations of the clamp that were more rigid so that it deformed less when we tightened the quick release and that were of different geometries such that they released the tubes better. Because they are easy to make, we fabricated two designs, a clamp that was hinged top-bottom and a clamp that was hinged left-right. Through empirical testing we found the left-right split clamp to best meet our design goal of being easy to use.

After deciding on our seat clamp, we realized that the chain path interfered with the seat when the bike was in the highest gear and the seat was in the rearmost required position. To address this we looked for a solution that would require little machining and maintain a low seat profile and high drive train efficiency. We discussed several options: raising the seat, trimming the seat clamp on the chain side, cutting a clearance notch in the chain side of the seat, and adding an idler. In order to fully ensure that the chain would not contact the seat, we combined the first three options into our modification, as shown in the figure below.

For the prototype, we made the seat out of wood because wood is light and relatively easy to fabricate. We considered several material options for the final vehicle, including fiberglass, plastic, and wood. Fiberglass would create a beautiful molded seat, but would require considerably more time and effort to produce than simpler designs. For plastic, we were unsure of exactly how we could build the seat in a way that would be rigid enough for competition riding. Wood provided the best option, as we could cut it and form it to our specifications with tools that we already possessed. This year we used poplar instead of particleboard; our seat strength is superior and the appearance is aesthetically pleasing.

2.5 ROLL BAR DESIGN

In designing the roll bar, our main concern was that it be able to withstand the required loading conditions. However, we also wanted to make the frontal area and internal configuration of our vehicle as compact as possible while still allowing all riders to fit within the roll bar. To minimize frontal area we wanted to place the roll bar behind the rider so that it was just wider than our widest rider's shoulders, thus still providing necessary protection but minimizing the roll bar's contribution to frontal area. However, because of our reclined seating position, the rider's shoulders are the farthest aft point on his or her body. A completely vertical roll mounted on the main frame tube necessitates a long frame, but if we could angle the roll bar somehow, the frame could be shortened while still keeping the narrow roll bar behind the rider.

We considered a number of possible solutions to this dilemma, of which the main ones were an angled roll bar, a roll bar mounted on the rear fork, and an out-of-plane roll bar. Both the out-of-plane roll bar and the one mounted on the rear fork were rejected because our computer analysis showed dangerous stresses (see Section 2.3). The roll bar mounted on the main frame and angled to the rear satisfied the structural requirements and allowed us to make the roll bar as narrow as possible while still protecting the rider.

2.6 FAIRING DESIGN

FAIRING SHAPE IDEATION

Fairing ideation began with several main goals: to produce an aerodynamic shape that completely enclosed the vehicle and rider, was aesthetically pleasing, and designed for ease of manufacturing. This last constraint was initially very limiting because we devised an innovative construction method described below, resulting in shapes such as Fairing F in Figure 4, which are defined entirely as simple geometric shapes (elliptical cylinders, ellipsoids, etc). An improvement to our mathematical engine enabled use of splines and more complex fairing shapes.

Overall, our design process involved idea generation by making lots of different fairing shapes, refining them to best suit our goals, and producing a set of different shapes that could be analyzed by FEA tools to make a final decision based on which shape best met our goal of an aerodynamic shape. The refining of a single design can be seen in Fairings A, B, and C, which were derived from the same initial shape with subtle differences to modify the outward appearance of the shape or the internal space available for the rider. We did not structure the fairing design as rigorously as the design of the frame, for example, because in general the fairing does not lend itself as well to such a design process. We also felt that our focus on reliability and our goal of producing a full composite fairing necessitated focusing our efforts on the construction of a fairing, so we could practice riding a fully faired vehicle, rather than on the subtleties of the fairing's aerodynamics and design.

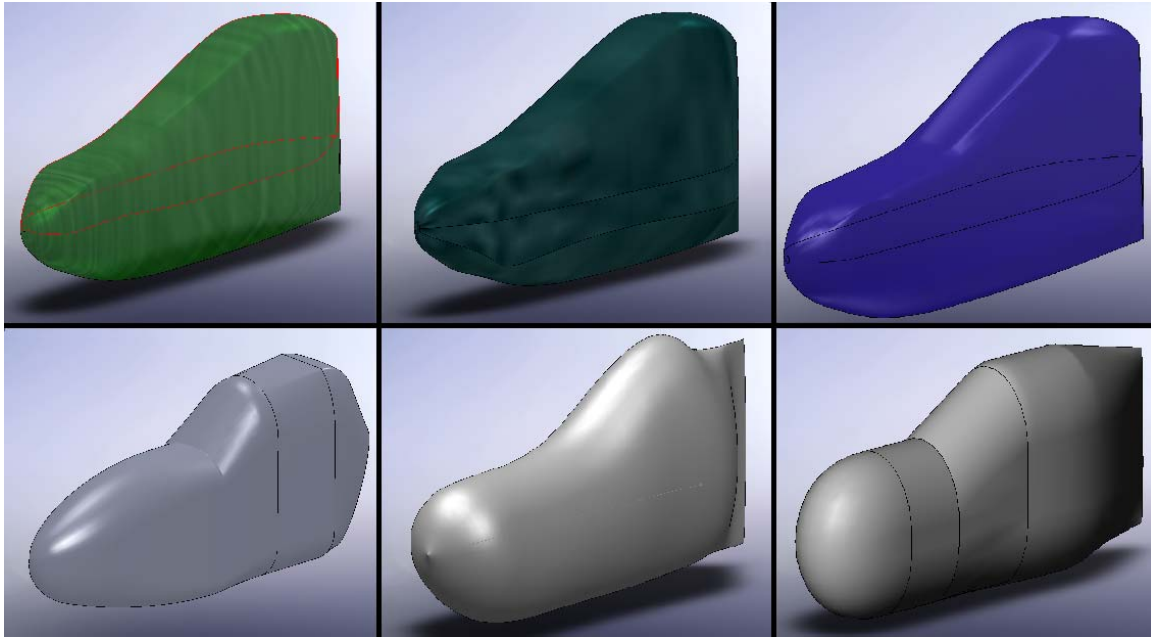


FIGURE 4: FAIRING CONCEPTS PRODUCED BY INITIAL DESIGN PROCESS. DESIGNS REFERENCED AS FAIRINGS A THROUGH F GOING LEFT TO RIGHT, TOP TO BOTTOM.

Figure 4 shows the set of fairing shapes we presented for CFD analysis. Some have obvious aerodynamic deficiencies, but the set of 6 shapes is representative of the results of our design process and we chose to rely on the results of our analysis of these shapes to help us choose a final design for our fairing.

FAIRING CONSTRUCTION TECHNIQUE

In the past we have constructed the composite sections of our fairing by building a large positive mold from blue foam, building up an oversized foam shape then sanding it down to match the CAD model of our fairing. With proper finishing of this mold, fiberglass can be laid up on the outside of this mold and used either as a female mold for the final shape or as the final shape itself, depending on the desired surface finish. This technique requires considerable time and expense in mold making; limited resources drove us to seek out alternative construction methods for the fairing. Certainly there are numerous mold making techniques, but what if we didn't have to make a mold? We discovered a surfboard maker in California who uses a lattice of notched cardboard pieces covered in fiberglass to produce cheap, lightweight surfboards (Sheldrake, 2009). Several of our members sought to apply this novel technique to fairing construction.

All of our CAD design of the fairing was done in SolidWorks, using lofts to produce solid bodies from two dimensional guide curves and cross sections. These guide curves can be either made up of dimensioned geometric components (i.e. straight lines, conic sections, etc) or splines, which are smooth curves generated between control points. The curvature and fine detail of splines can be adjusted by adding additional points or modifying the spline's control polygons, a polygon shape defined between every pair of points in a spline. This polygon contains two additional points that are used mathematically to define the curvature of the spline by specifying the first derivative (or slope) of the spline as it passes through the control points. Solidworks stores the location of all the control points in a spline as well as the additional points for each control polygon; accessing this information allows one to extract and reproduce the spline mathematically. For a fairing shape defined by splines, doing this for each of the three guide curves (actually four, but fairings are symmetrical side-to-side) as well as the cross sections (defined as perpendicular to the long axis of the fairing) enables complete reproduction of the Solidworks

shape mathematically. Using MATLAB, we created a program that takes all the spline and cross section information from Solidworks and will return a point on the fairing shape when interrogated with a vector projected from the long axis of the fairing.

With a fairing shape defined mathematically, the next step is building the lattice structure for that shape. The surfboard maker uses three sets of interlocking cardboard pieces to produce a lattice. For a surfboard this lattice is basically planar, but a fairing is a hollow, semi-cylindrical shape. If one wraps this lattice around on itself, it produces a cylinder made of circular ribs and two sets of spars wrapping around the cylinder, one clockwise and the other counterclockwise. This cylinder can be defined mathematically in cylindrical coordinates based on the desired density of spars and the angle of the spars from the long axis of the cylinder. Combining the fairing shape defined previously with this cylinder in a MATLAB script, by stretching the cylinder along the long axis of the fairing shape, the lattice can be projected outward onto the fairing shape. Tweaking several resolution parameters affecting linear and angular spacing, rays can be projected from the long axis of the fairing perpendicularly outward through the lattice on the cylinder and then the rays' intersection with the fairing shape is recorded. In this way the lattice is projected onto the fairing shape.

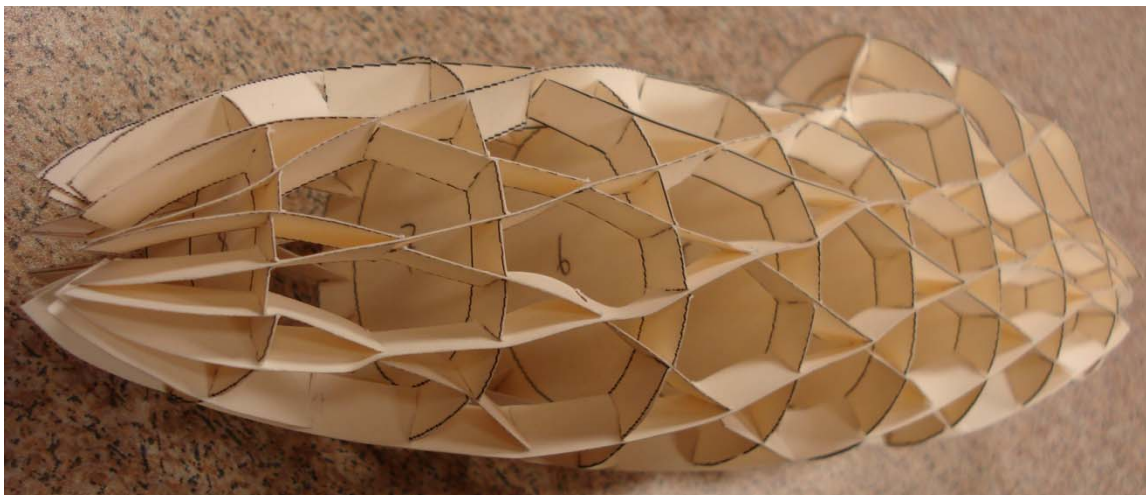


FIGURE 5: A SMALL SCALE MODEL DEMONSTRATING OUR LATTICE-GENERATING PROGRAM AND CONSTRUCTION METHOD.

The program collects the coordinates of the intersection points for each rib and spar of the lattice. These points for the ribs are plotted and connected to give the shape of the rib. This shape is offset by some defined width to produce a hollow rib shape. Based on the predefined angular frequency of spars, marks are added to the rib plot to note where notches will need to be cut to interlock with the spars. The points from the projection of each spar are similarly plotted; beginning at the origin, each point projected on the fairing is laid down to form a two dimensional plot of the spar, using a trigonometric conversion to account for the curvature of the three dimensional shape. The width of the spar is then added and notches are marked. The ribs are the first parts of the assembled lattice so all their notches are on the outside of the rib. Clockwise spars are added to the assembly next, so they have interior notches for intersection with the ribs and exterior notches for joints with the counterclockwise spars which are added last. Each rib and spar plot also gets a sizing line that can be measured after printing to ensure proper scaling of the part. The program exports these plots of each rib and spar as two image files which can be manipulated as necessary for printing. The printed outlines can then be transferred to cardboard, cut out, and assembled into the fairing (as shown in Figure 5), ready for fiberglass.

3 ANALYSIS

3.1 FRAME ANALYSIS

We began frame analysis by determining the center of mass of each member of our team with regard to the vehicle. We then created a mass-weighted average location for the center of mass. To do so, we placed a scale under each wheel of the vehicle and weighed each team member as they sat in their riding position. This was done first on a horizontal surface, so we could find the center of mass in x. We then placed the front tire above the rear and took the same measurements, which we used to find the center of mass in y.

Taking these values, we then wrote a script in MATLAB that finds the weighted average center of mass of the riders. Using the dimensions of the CAD model, the results are scaled and plotted onto a basic frame shape for reference.

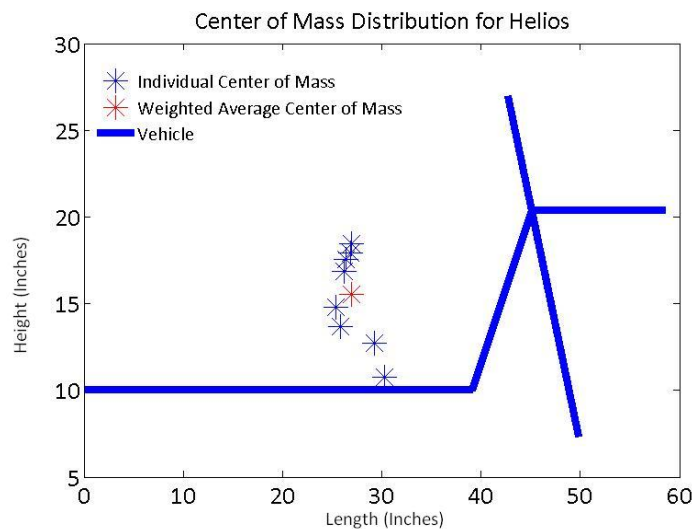


FIGURE 6: CENTER OF MASS DISTRIBUTION FOR OUR RIDERS ON HELIOS.

As seen in Figure 6, the center of mass for two of the riders is too low, below that of the seat. However, the other values, including the average value, are within an acceptable range, indicating that the error is likely due to experimental error rather than to computation. Using the center of mass, we can determine accurate loading conditions for the vehicle using ANSYS.

Analysis was done initially to determine our maximum possible deceleration while maintaining contact between the wheels and the ground. We know maximum braking occurs when our resultant acceleration vector points from our center of mass to the contact point of the front wheel. Beyond this, we will start to tip over forward. Based on the angle between the center of gravity and the center of gravity, if we assume that the only vertical acceleration is that due to gravity, the maximum braking force is 1.42G. In real terms, this means that from our maximum speed of 45mph, we would take 47ft to stop, and we would stop in about 1.5sec. This is a good stopping distance. However, our experience from last year indicates this may be a shortsighted estimate: in a situation where immediate maximum braking is required, steering control and other critical factors such as driver reaction and wind could cause undesired behavior regardless of ideal braking behavior.

In addition to maximum deceleration, we wanted to identify areas of possible failure in the frame. To do this, the frame geometry was imported into ANSYS from SolidWorks, and analysis was conducted using shell elements. After determining the location of the center of mass of our riders, we decided on a worst-case loading scenario. We assumed our riders weighed 200lbs. In terms of accelerations, a 3G bump occurring with severe 0.75G braking was applied. The 3G bump is an industry standard (Carroll, 2003), while the 0.75G bump is that required

to stop from 15mph in 10ft. This loading was applied to the frame as a remote load, where the force acted at the center of mass and was applied to the frame at a point below the center of mass. The front of the vehicle was constrained about an axle, such that it was constrained in the vertical and horizontal direction – the axle could rotate, but its axis would remain fixed. This process of fixing the front axle is standard industry practice (Vandermark, 2009). The rear axle was constrained only in the y axis, and free in x and all rotational degrees of freedom. This corresponds to loading conditions on an actual frame – the distance between the axels changes, and constraining it results in improper simulation results.

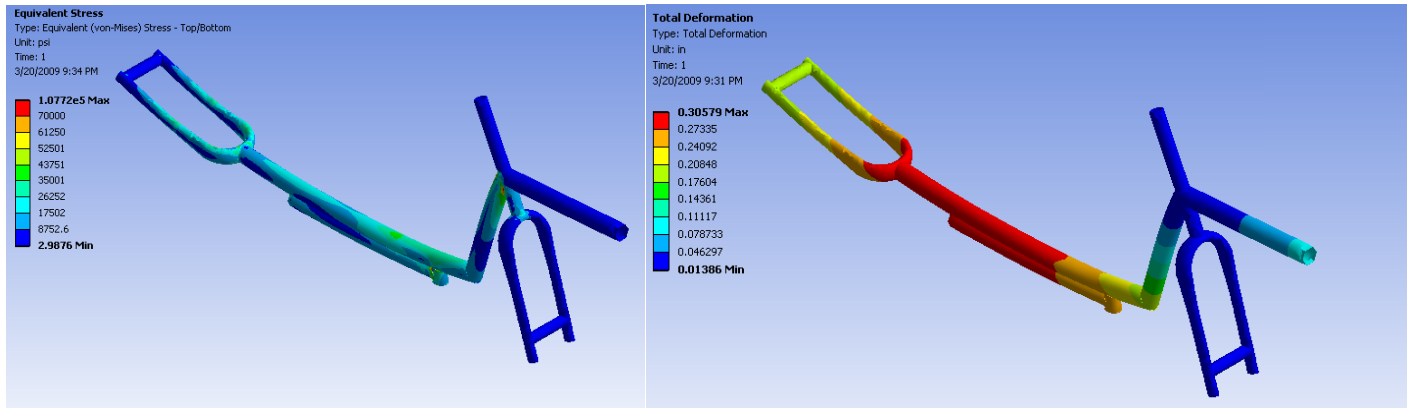


FIGURE 7: LEFT SHOWS THE EQUIVALENT STRESS FOR OUR INITIAL FRAME. RIGHT SHOWS THE DISPLACEMENT PLOT. OVERALL, NO LARGE AREAS OF STRESS ARE PRESENT, AND THE DISPLACEMENTS ARE REASONABLY SMALL.

The result of our analysis can be seen Figure 7. The maximum displacement is slightly more than 0.25in. However, the vertical displacement, what is most important and most felt when riding the vehicle, is only 0.1in. Overall, the stress is generally at acceptable levels. The simulation indicates stress concentrations at a few points – most notable around the interchange and at the intersection of the head tube and slant tube (see Figure 8). The stress concentration at the interchange appears to be partly an artifact of the finite element method. Furthermore, it occurs at a location that will have a significant weld bead, distributing the load around more metal and reducing the stress. At the head tube, there are two locations of high stress concentration – at the bottom and top of the joint. While the stress at the bottom of the joint could be dealt with by a weld bead, the high stresses seen at the top of the joint may not, and alternative means were necessary to reduce this stress.

We investigated the use of a gusset to redistribute this stress more evenly along the tube. Our initial was a set of solid, triangular sheets mounted tangentially to the joint, as seen in Figure 9. These were not functional. While they do reduce the stress at some points in the tube, they raise it in other areas, causing stress concentrations. In order to solve this, a series of holes were placed in the gussets. As you can see, the placement of the holes reduced the magnitude of the stress concentrations, and reduced the stress seen at the tube. It is especially encouraging that they are reduced at the area above the joint, in addition to below it. While there are still places where analysis indicates stress concentrations will be above the yield point of the metal, these are small and in weld zones. Additionally, the maximum stress has gone down below the ultimate strength. The welding bead will add metal, reducing stress. Also, if the stress concentration is small enough, as we expect it to be, the metal will yield in a ductile manner, re-configuring itself into a more stable geometry. It is also important to note that the stresses are all below the ultimate strength of steel, indicating that even though it may yield, once it has done so it will stay in that configuration and is in no danger of failing.

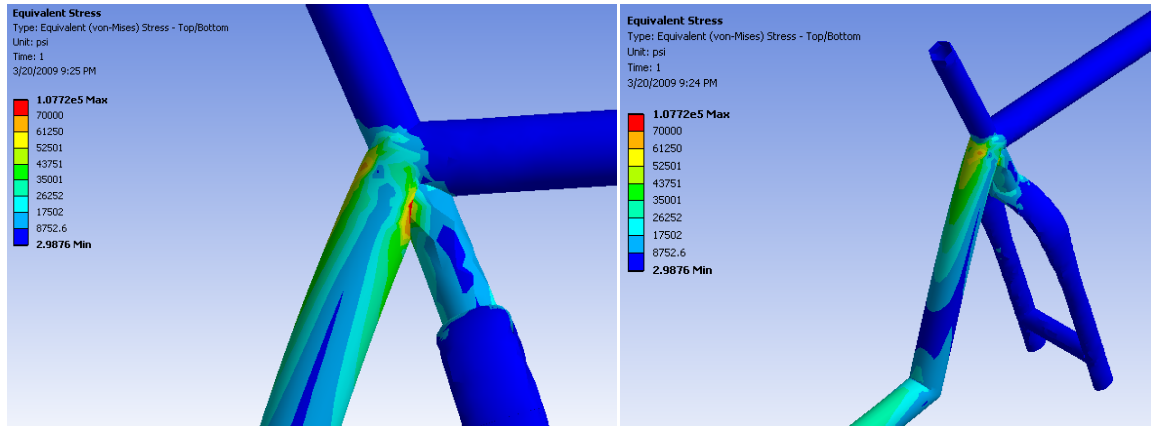


FIGURE 8: THE ORIGINAL, UNMODIFIED FRAME. NOTE HIGH STRESSES AT BOTH TOP AND BOTTOM OF THE SLANT TUBE NEAR THE JOINT.

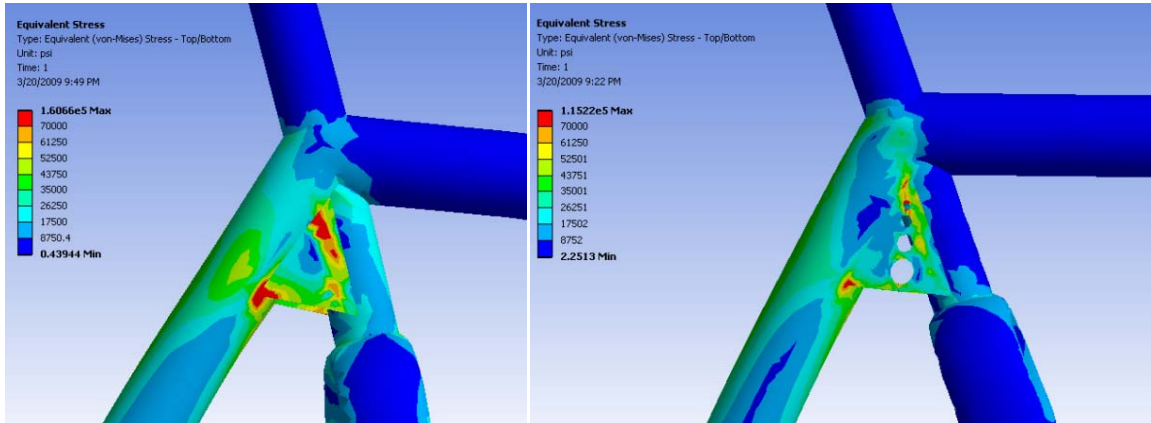


FIGURE 9: THE UNMODIFIED GUSSET IS SEEN AT RIGHT – NOTE LARGE AREAS (INDICATED IN RED) THAT ARE ABOVE THE YIELD STRENGTH OF OUR MATERIAL. AT RIGHT, THE STRESS IS LOWER OVERALL AND MORE EVENLY DISTRIBUTED ACROSS THE GUSSET. ALSO NOTE THE LOWER MAXIMUM STRESS VALUE.

3.2 FAIRING ANALYSIS

Initially, six possible fairing shapes were designed; each fit the vehicle entirely and provides good visibility and room for each rider. The aerodynamic analysis of each fairing would help to show which design would provide the best performance in competition. The aerodynamic fairing analysis was performed in SolidWorks COSMOS FloWorks in order to visualize the pressure gradient on the fairings' surfaces, velocity of fluid around the fairing, and to calculate the C_dA . Each fairing was evaluated with the same testing conditions, using an 18m/s wind speed. It is important to note that for all analysis, the effect of drag on the wheels was ignored to simplify the model. Due to the comparative nature of the analysis and the consistent placement of the wheels for each model, this assumption should not hinder the results.

The analysis for each fairing showed similar surface pressure and external air velocity behavior. In surface pressure, a high pressure zone is present at the nose portion of each design. Traveling towards the peak of each fairing, another high pressure zone is present on the canopy region. These two high pressure zones are a directly caused by the frontal cross sectional area of the fairing. Once hitting the peak of the shape, the air pressure drops creating a low pressure region. Overall the high and low pressures are shown to be at 101500Pa and 101100Pa, respectively. It is not surprising that each fairing shape had this overall pressure profile. Each fairing uses the

canopy style design, for increased visibility, resulting in this pressure pattern. These pressure profiles can be seen in Figure 10 for a few of fairing concepts.

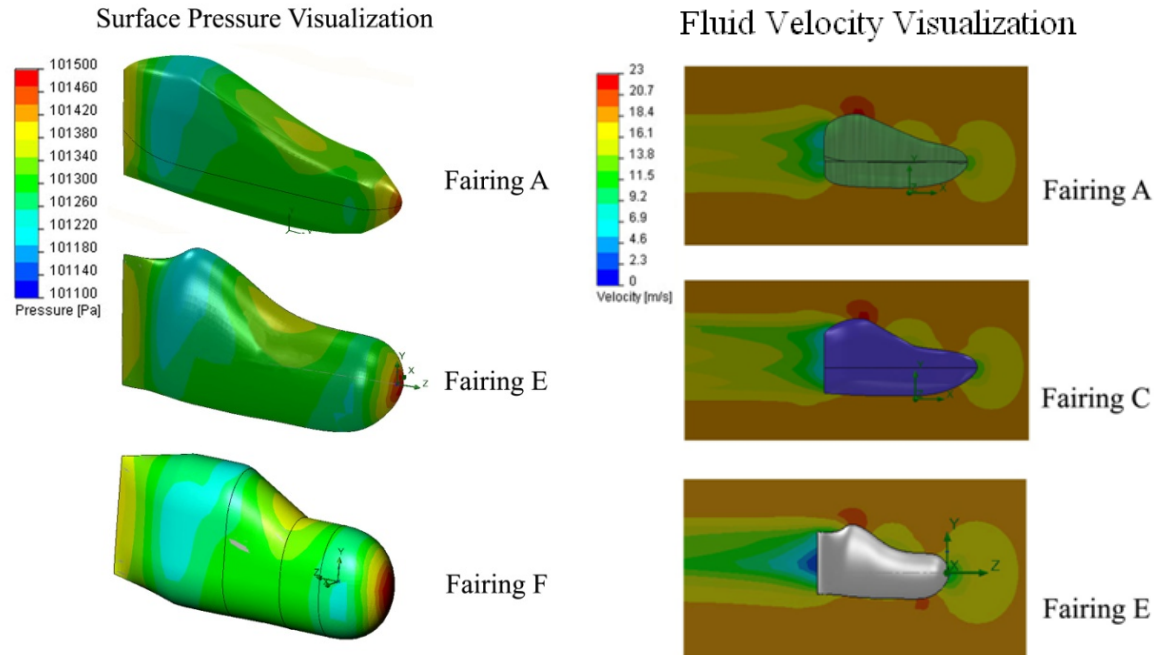


FIGURE 10: LEFT DEPICTS THE SURFACE PRESSURE OF THREE OF THE SIX FAIRING CONCEPTS. EACH FAIRING HAS THE SAME OVERALL PRESSURE PROFILE, WITH SLIGHT VARIATIONS IN PRESSURE REGION SIZES AND VALUES. RIGHT SHOWS THE VELOCITY OF THE AIR AROUND EACH FAIRING SHAPE. SIMILAR TRENDS CAN BE SEEN IN CASES NOT SHOWN ABOVE.

As seen with the surface pressure, the overall trend for external fluid velocity is the same for each design. Low velocity regions are found at the nose cone, canopy area, and at the tail box. The highest velocities are found at the peak of each design, probably due to more turbulent air flow. The analysis reports the highest velocities to be about 23m/s. These velocity profiles can also be seen in Figure 10.

Because each design had similar surface pressure and fluid velocity behaviors, the C_dA calculation would provide more quantitative distinction. Using the expression,

$$F_D = \frac{1}{2} \rho C_D A v^2$$

for aerodynamic drag force (Wikipedia), the C_dA for each shape was calculated. The density of the air was taken to be 1.184kg/m^3 (Wikipedia) and the velocity of fluid to be 18m/s . We computed the drag force from the results of the FloWorks analysis. Table 5 shows the drag force and C_dA results for each design.

| | Drag Force (N) | C_dA (m^2) |
|------------------|----------------|-------------------------|
| Fairing A | 6.105 | 0.0318 |
| Fairing B | 6.295 | 0.0328 |
| Fairing C | 6.412 | 0.0334 |
| Fairing D | 14.278 | 0.0744 |
| Fairing E | 22.833 | 0.119 |
| Fairing F | 16.326 | 0.0851 |

TABLE 5: $C_D A$ CALCULATIONS FOR FAIRING CONCEPTS. THE $C_D A$ FOR EACH OF THE SIX FAIRING CONCEPTS WAS CALCULATED FOR QUANTITATIVE COMPARISON.

The $C_D A$ calculation shows that Fairing A, with the lowest value 0.0318m^2 , would have the best aerodynamic performance in comparison with the other concepts. Based on these results, we chose the final fairing concept to be Fairing A, which is shown Figure 11.

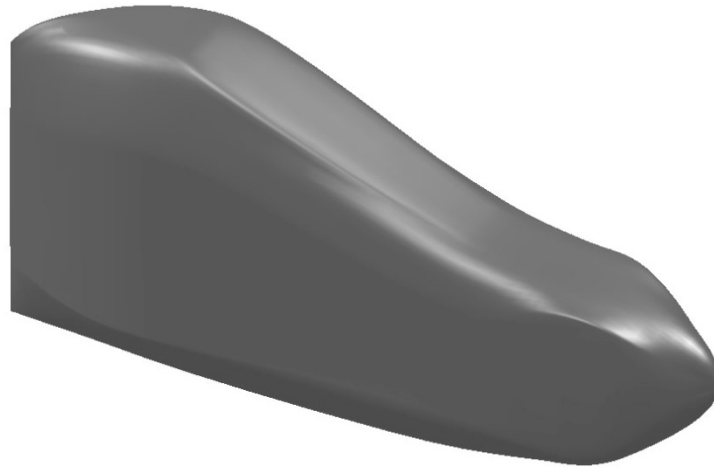


FIGURE 11: FINAL FAIRING CONCEPT. THE FAIRING A DESIGN HAD THE LOWEST $C_D A$ VALUE, AND WILL BE PURSUED AS THE FINAL FAIRING DESIGN.

Compared to past vehicles' fairing concepts, this fairing is not as aerodynamic, which is to be expected with the increased seating angle. The 2007 vehicle, *Aurora*, had a $C_D A$ of 0.021m^2 , and the 2008 vehicle, *Vega*, 0.014m^2 . With the increased fairing angle and size a $C_D A$ value of 0.0318m^2 seems reasonable for this design. Though the aerodynamic characteristic of the *Helios* fairing is not as good as past designs, the tradeoff is for increased visibility and overall vehicle stability.

3.3 ROLL BAR ANALYSIS

Our roll bar is central to the *Helios's* Rollover Protection System and, as such, must be made to withstand the maximum load expected in a crash situation. For this competition this loading condition is specified as two load cases: a top load of a 600lb force applied to the top of the roll bar at 12° from vertical towards the aft of the vehicle, and a side load of 300lbs was applied horizontally at shoulder height. While ultimate strength is important, deflection of the roll bar under load is also a concern because too much deflection could mean the roll bar won't protect the rider during a crash. With the top loading conditions there should be less than 2in of deformation and with the side load conditions the frame and roll bar should have less than 1.5in of elastic deformation. In neither case should the roll bar contact the rider's head or helmet in the deformation process.

Analyzing our roll bar, we took dozens of different designs from our initial design phase and analyzed them in ANSYS Workbench. We imported CAD models of the roll bars and frames from SolidWorks into ANSYS Workbench, where material properties of the tubes were specified. The model of the frame was simplified from the full frame to a small section of the frame around the rear fork, which made the analysis faster but limited the usefulness of these results to simply comparing different roll bar geometries. Analysis of the frame as a whole was done separately. We applied loads and boundary conditions to the roll bar to satisfy the design requirements and mimic the conditions in which we would be testing the roll bar.

Our first roll bar iteration involved a completely vertical roll bar with no support bars. Without the support bars the roll bar's deformation was much higher than the maximum allowed. The addition of support bars reduced the deformation, but the roll bar still needed to be moved aft to allow us to shorten the main frame tube and keep the vehicle compact. Two of the solutions investigated are shown in Figure 12.

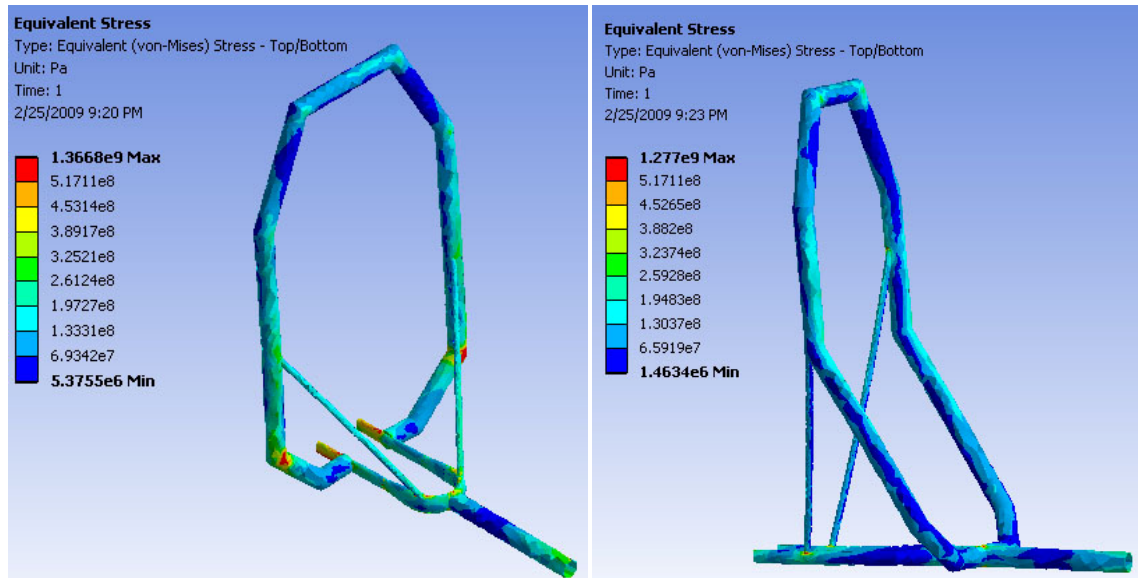


FIGURE 12: EQUIVALENT STRESS FOR SEVERAL ROLL BAR DESIGNS UNDER THE 600LB TOP LOAD. LEFT IS A VERTICAL ROLL BAR MOUNTED ON THE REAR FORK AND RIGHT IS AN OUT-OF-PLANE DESIGN MOUNTED ON THE MAIN FRAME TUBE.

For the design above that places the support bars in compression (the out-of-plane design), we were worried that the support bars would buckle, so we used Euler's buckling equations to calculate the critical forces that would cause the bars to buckle. Using the buckling equation,

$$F = \frac{\pi^2 EI}{(Kl)^2}$$

where F is the critical buckling load, we found the static buckling load for a 24in length of steel tubing for the support bars to be:

$$\frac{\pi^2 * 30e6 * .00306}{(0.8 * 24)^2} = 2457.76lbs.$$

This result says that the roll bar can support 2458lbs of static force before buckling. In a crash situation, the loads will be applied dynamically, so this static buckling result is, at best, an estimator of the load under which these supports will fail and the result should be taken lightly. However, the Euler buckling equation has most pessimistic boundary constraints for these loads and we believe this result demonstrates that support bars of approximately 24in are safe from buckling.

Both of the designs shown in Figure 12 have serious weaknesses. The roll bar mounted on the rear fork places high stresses on the rear fork and we had serious concerns about welding the large 1.5in tubing of the roll bar to the much smaller tubes of the fork. The out-of-plane roll bar was attached to the main frame tube so stress on the rear fork was reduced, but welding of the out-of-plane tubes would be considerably more difficult than a planar design. We began to investigate simple, angled back roll bars at several different angles. We considered roll bars at angles

of 10°, 15°, and 20° from vertical with support bars to the rear fork. When analyzed, the deflection of 20° design far exceeded the allowable value of 2in under the 600lb top load. The 15° design was within the allowable limit under the top load, but the side load of 300lbs deformed the roll bar beyond 1.5in, as shown in Figure 13.

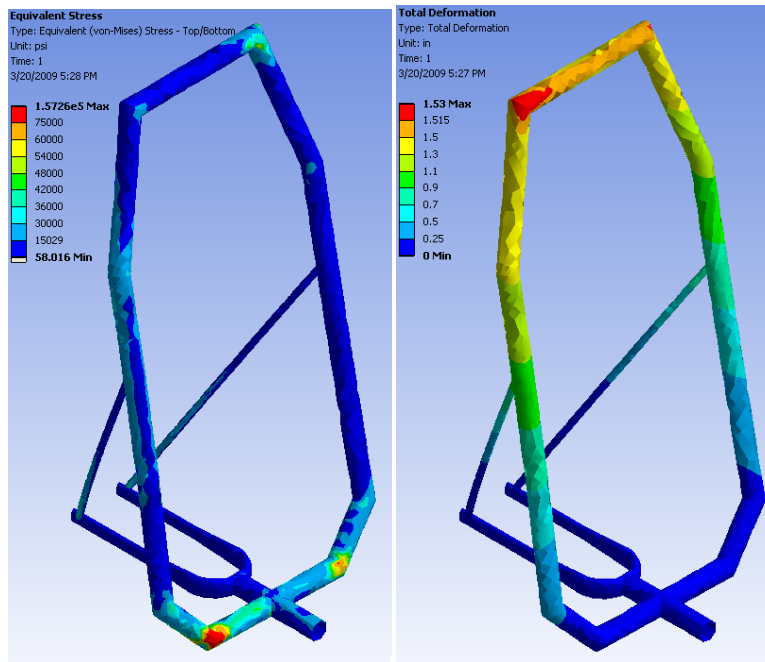


FIGURE 13: EQUIVALENT STRESS (LEFT) AND TOTAL DEFORMATION (RIGHT) FOR THE 15° ROLL BAR UNDER 300LBS SIDE LOAD.

Because the more steeply angled roll bars failed to meet the design requirements for deformation, we analyzed a 10° roll bar of a similar design. The results of the analysis of this design under the 600lb vertical load are shown in Figure 14. Deformation under this load was well within the allowable, at a maximum of 1.24in. Equivalent stress was generally low, with several notable concentrations around the joint between the support bars and the roll bar. However, these concentrations were localized and are artifacts of the finite element analysis; the weld bead joining the supports to the roll bar will dissipate these concentrations.

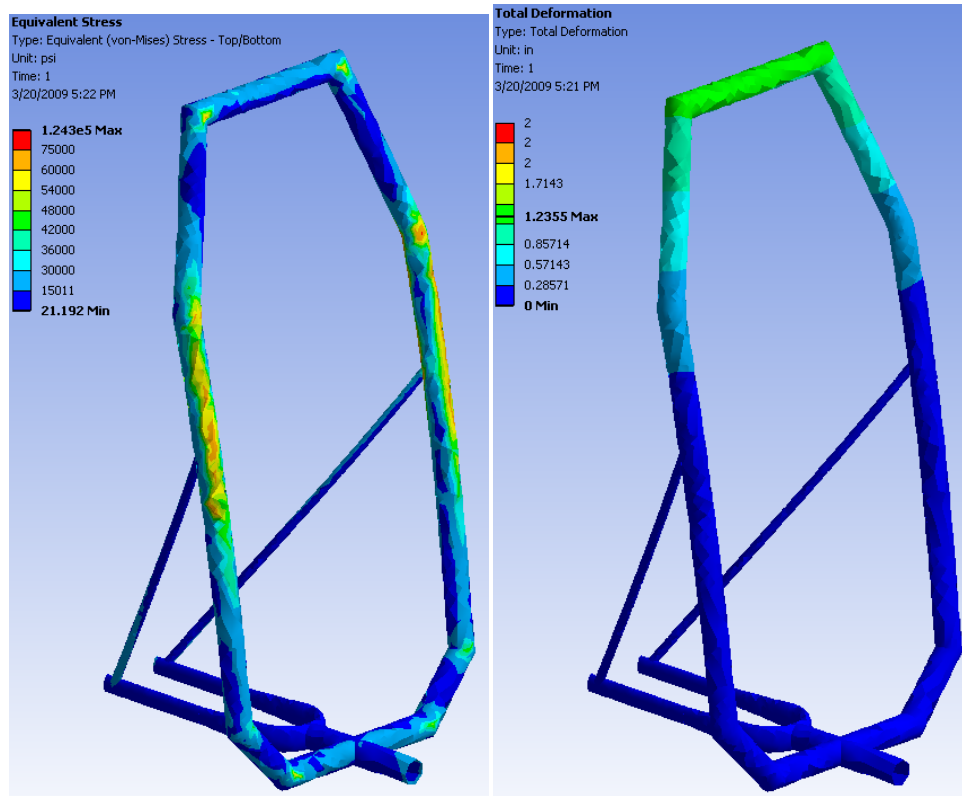


FIGURE 14: EQUIVALENT STRESS (LEFT) AND TOTAL DEFORMATION (RIGHT) FOR THE 10° ROLL BAR UNDER 600LBS TOP LOAD.

Similarly for the 10° roll bar design under the 300lb side load, total deformation was within the allowable limit of 1.5in and equivalent stress generally low. The moment about the joint at the main frame tube creates high stresses in the lower joints of the roll bar. These concentrations are located right at the joint, where weld beads will be distributing the stress, eliminating the concentrations and reducing stress to allowable levels.

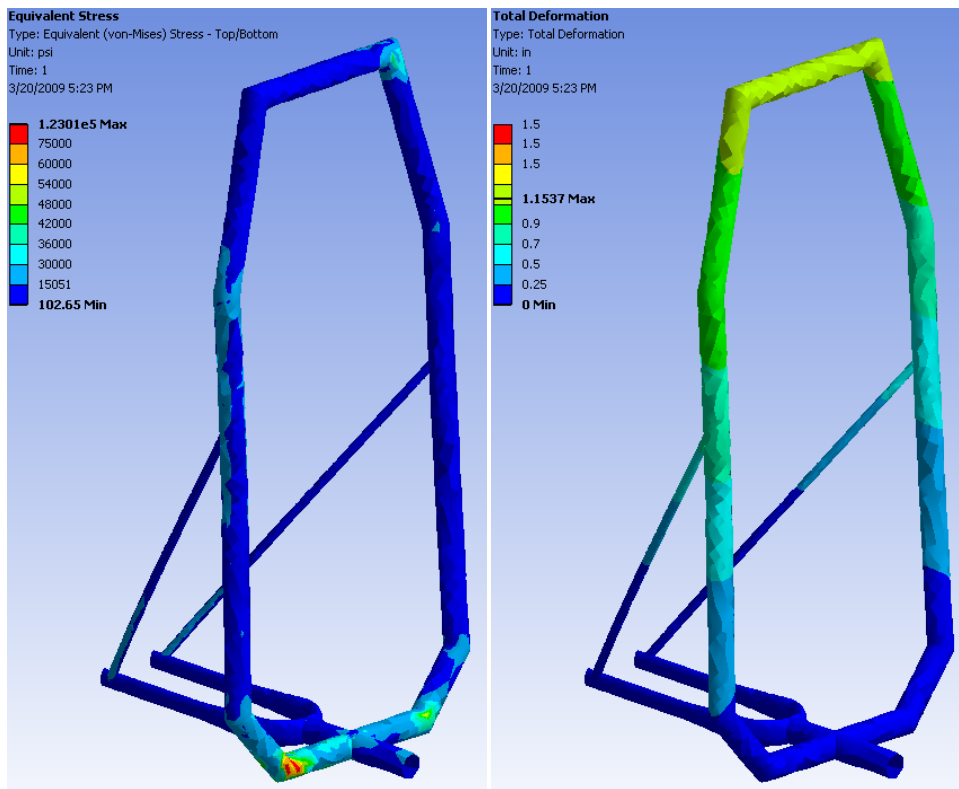


FIGURE 15: EQUIVALENT STRESS (LEFT) AND TOTAL DEFORMATION (RIGHT) FOR THE 10° ROLL BAR UNDER 300LBS SIDE LOAD.

Based on the results of our finite element analysis of different roll bar designs we selected a planar roll bar angled 10° aft as our final roll bar design. This angle will allow us to shorten the frame and bring the rear wheel in towards the rider, while still keeping the roll bar behind the rider.

3.4 DRIVETRAIN ANALYSIS

All supports or other structures associated with the drivetrain were considered part of the frame for purposes of finite element analysis, and detailed discussion and interpretation of this analysis can be found in the Frame Analysis section. Additionally, all of the drivetrain components that will be used in the *Helios* will be stock, commercially-available components which we assume to be structurally sufficient for use in our drivetrain. This leaves only one aspect of the drivetrain in need of detailed analysis: the sizing of sprockets to achieve an appropriate range of gear ratios for competition.

Based on the values of sprockets chosen during design of the drivetrain, we set up a simple spreadsheet program to take in important drivetrain component sizes, such as sprocket sizes and rear wheel diameter, and calculate the vehicle's speed for each possible gear combination at different pedal cadences. The drivetrain is composed of two chains, one linking the crankset to the interchange and the other connecting the interchange to the rear cassette. For the rear cassette we chose to use a 9-speed off-the-shelf cassette to provide a wide range of gear ratios, with sprocket sizes from 11 to 34 teeth. Initial analysis with our spreadsheet indicated the need for an additional gear reduction at the interchange, even when the largest commercially-available crankset sprockets were used (53 or 54 teeth).

Without the additional reduction our top speed (at a cadence of 120rpm) would be about 33.5mph, far below the 45mph mark set during the initial design phase. Requiring different sized sprockets at the interchange actually

simplified the design of the drivetrain, enabling use of a standard right crank with the crankarm removed and mounted on a standard bottom bracket as a mount for the interchange gears. A right crank typically holds two or three sprockets for use with a front derailleur but in this case we saw an opportunity to use one to hold two appropriately sized sprockets for the gear reduction we required. Using the spreadsheet and constrained by commercially-available components, we settled on a 22 tooth inner sprocket (connected to the crankset) and 36 tooth outer sprocket (connected to the rear cassette). This combination enables us to reach our 45mph design point in the second-to-highest gear at 120rpm (as shown in Table 1) or in the highest gear at 100rpm, a more reasonable cadence for our less experienced riders.

| | | | SPROCKET (teeth) | RATIO | LOW SPEED (mph) | MID SPEED (mph) | HIGH SPEED (mph) |
|----------------------|------|-------|---------------------|-------|--------------------|--------------------|---------------------|
| CRANKSET | 53 | teeth | 34 | 2.55 | 11.84 | 14.80 | 17.76 |
| INTERCHANGE 1 | 22 | teeth | 30 | 2.89 | 13.42 | 16.77 | 20.13 |
| INTERCHANGE 2 | 36 | teeth | 26 | 3.34 | 15.48 | 19.35 | 23.22 |
| WHEEL DIA. | 19.5 | in | 23 | 3.77 | 17.50 | 21.88 | 26.25 |
| LOW RPM | 80 | rpm | 20 | 4.34 | 20.13 | 25.16 | 30.19 |
| MID RPM | 100 | rpm | 17 | 5.10 | 23.68 | 29.60 | 35.51 |
| HIGH RPM | 120 | rpm | 15 | 5.78 | 26.83 | 33.54 | 40.25 |
| | | | 13 | 6.67 | 30.96 | 38.70 | 46.44 |
| | | | 11 | 7.88 | 36.59 | 45.74 | 54.89 |

TABLE 6: OUR SPREADSHEET ANALYSIS, SHOWING DRIVETRAIN INPUTS AT LEFT AND SPEED RESULTS TO THE RIGHT

With appropriately-sized sprockets, the drivetrain in its highest gear will ideally give a vehicle top speed of about 45mph, the fastest any vehicle in this competition has ever gone. We may not actually be able to go that fast in competition, but the record makes a reasonable design point for our vehicle. Additionally, the drivetrain should provide a range of lower gear ratios for acceleration up to maximum speed and for the slower endurance event. Due to space constraints, the sprocket sizes at the interchange, which sits between the rider and the ground, need to be minimized to provide space for the fairing. With these basic requirements we began to investigate commercially-available components that could meet our needs.

3.5 VEHICLE COST ANALYSIS

| <i>Single Vehicle Cost Estimation</i> | | | | | |
|---------------------------------------|-------------------------------|----------|-----------|------------|------------|
| | Description | Quantity | Unit Cost | Units | Total |
| FRAME | | | | | |
| 1 | Thin Walled 4130 Steel Tubing | 8 | \$7.20 | Per Foot | \$57.60 |
| 2 | Welding Supplies | 1 | \$20.00 | Lump Sum | \$20.00 |
| 3 | 4' x 8' Sheet, Plywood | 1 | \$20.00 | Per Board | \$20.00 |
| 4 | Aluminum Blocks | 1 | \$30.00 | Lump Sum | \$30.00 |
| 5 | Assorted Hardware | 1 | \$60.00 | Lump Sum | \$60.00 |
| | | | | Subtotal | \$187.60 |
| FAIRING | | | | | |
| 6 | Epoxy | 10 | \$60.00 | Per Gallon | \$600.00 |
| 7 | Fiberglass, 6 oz. | 20 | \$25.00 | Per Yard | \$500.00 |
| 8 | Kevlar, 10 oz. | 2 | \$50.00 | Per Yard | \$100.00 |
| 9 | Cardboard for Honeycomb | 2 | \$29.25 | Per Sheet | \$58.50 |
| 10 | Assorted Composites Tools | 1 | \$50.00 | Lump Sum | \$50.00 |
| 11 | PETG (8' x 4') | 1/4 | \$70.90 | Per Sheet | \$17.73 |
| | | | | Subtotal | \$1,326.23 |

| DRIVETRAIN | | | | | |
|-------------------|---------------------------|---|----------|-------------------|-------------------|
| 12 | Derailer | 1 | \$100.00 | Per Unit | \$100.00 |
| 13 | Wheels | 2 | \$100.00 | Per Wheel | \$200.00 |
| 14 | Front Crankset | 1 | \$50.00 | Per Unit | \$50.00 |
| 15 | Chains | 2 | \$20.00 | Per Unit | \$40.00 |
| 16 | Interchange Sprockets | 2 | \$15.00 | Per Unit | \$30.00 |
| 17 | Pedals | 1 | \$75.00 | Per Set | \$75.00 |
| 18 | Brakes | 1 | \$50.00 | Per Set | \$50.00 |
| | | | | Subtotal | \$545.00 |
| SEAT | | | | | |
| 19 | Poplar Board | 1 | \$17.00 | Per Board | \$17.00 |
| 20 | Stain | 1 | \$4.97 | Per Can | \$4.97 |
| 21 | Wood Screws | 1 | \$10.00 | Per Box | \$10.00 |
| 22 | Aluminum Plate for Clamps | 2 | \$40.00 | Per Plate | \$80.00 |
| 23 | Sanding Supplies | 1 | \$5.00 | Lump Sum | \$5.00 |
| | | | | Subtotal | \$116.97 |
| | | | | Total Cost | \$2,175.80 |

TABLE 7: COST ESTIMATE FOR CONSTRUCTION OF SINGLE VEHICLE.

| <i>Production Vehicle Cost Estimation</i> | | | | | |
|---|---------------------------------------|----------|------------|----------------------|--------------------|
| | Description | Quantity | Unit Cost | Units | Total |
| LABOR | | | | | |
| 1 | Machinist/Welder | 1 | \$4,000.00 | Per Month | \$4,000.00 |
| 2 | Composite Technician | 1 | \$5,000.00 | Per Month | \$5,000.00 |
| 3 | Manager | 1 | \$5,000.00 | Per Month | \$5,000.00 |
| | | | | Labor Total | \$14,000.00 |
| BIKE COSTS | | | | | |
| | Cost Savings Factor for Bulk Purchase | --- | 0.5 | | |
| 5 | Frame Jig | 1 | \$25.00 | Lump Sum | \$25.00 |
| 6 | Drivetrain Components | 10 | \$272.50 | Per Bike | \$2,725.00 |
| 7 | Frame | 10 | \$68.80 | Per Bike | \$688.00 |
| 8 | Fairing | 10 | \$663.11 | Per Bike | \$6,631.13 |
| 9 | Seat | 10 | \$58.49 | Per Bike | \$584.85 |
| | | | | Parts Total | \$10,653.98 |
| | | | | Total Cost | \$24,653.98 |
| | | | | Cost Per Bike | \$2,465.40 |

TABLE 8: COST ESTIMATE FOR PRODUCTION OF TEN VEHICLES PER MONTH. NOTE COSTS OF COMPONENTS ARE EQUAL TO SINGLE VEHICLE COST TIMES COST SAVINGS FACTOR.

4 TESTING

4.1 DRIVETRAIN EFFICIENCY

This year, we decided to construct a rear-wheel drive HPV after significant discussion and testing. To inform our decision, we measured the drive train efficiency of both last year's bike (front wheel drive) and this year's initial prototype (rear wheel drive).

To calculate the efficiency, we needed to find the total frictional torque added by the drive train. We assume this friction was mostly kinetic friction (independent of velocity) rather than viscous friction (velocity-dependent).

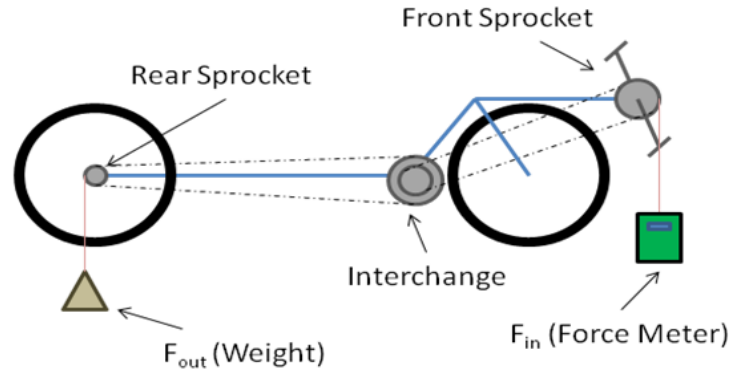


FIGURE 16: TEST SETUP - A WEIGHT IS ATTACHED TO THE REAR SPROCKET AND A FORCE METER TO THE FRONT SPROCKET. PULLING DOWN ON THE FORCE METER AT A CONSTANT VELOCITY AND MEASURING THE FORCE ENABLES ROUGH ESTIMATE OF EFFICIENCY.

We measured the frictional torque by a torque-balance technique (Figure 1). We wrapped strings around both the front and rear sprockets, and then placed a weight on the rear sprocket and a force meter on the front sprocket. We then pulled the force meter down at a constant velocity. The frictional torque was given by the following torque-balance equation,

$$\tau_{friction} = F_{in}R_{in} - F_{out}R_{out}G$$

where, R is radius and G is gear ratio (ω_{out}/ω_{in}). Efficiency is defined as the ratio of power out of the drive train to the power into the drivetrain. The efficiency is therefore,

$$\eta = \frac{\tau_{out}\omega_{out}}{\tau_{in}\omega_{in}} = \frac{F_{out}R_{out}G}{F_{in}R_{in}} = \frac{F_{in}R_{in} - \tau_{friction}}{F_{in}R_{in}}$$

Note how the efficiency is a function of the input force. Therefore, we estimated how much force our bikers could output at an average 75N.

We tested both *Vega* and the prototype and found that our new prototype was consistently more efficient, as shown in Table 9. Although last year's bicycle had less chain length, it lost power inside of its internal gear hub. The efficiency also drops dramatically when the front wheel is steered.

| Vehicle | F_{IN} (N) | F_{OUT} (N) | Friction Force (N) ($\tau_{friction}/R_{in}$) | Ideal Force Ratio (GR_{out}/R_{in}) | Efficiency |
|-----------------|--------------|---------------|--|--|------------|
| Vega (FWD) | 7.7 | 0.0 | 7.70 | 1.72 | 90% |
| | 19.6 | 6.9 | 7.70 | 1.72 | 90% |
| | 68.8 | 34.3 | 9.40 | 1.72 | 87% |
| Prototype (RWD) | 4.0 | 6.9 | 0.08 | 0.57 | 99% |
| | 17.8 | 24.2 | 4.00 | 0.57 | 95% |

TABLE 9: EFFICIENCY TESTING DATA FOR LAST YEAR'S VEGA AND THE CURRENT YEAR'S PROTOTYPE.

It is possible to alleviate all these efficiency problems with well-built front wheel drive HPV. For example, we could modify last's year bike design to use a cassette and chain guides. However, we decided that a rear-wheel drive system was easier to consistently attain good efficiency.

We made several assumptions in this efficiency test, many of which are unrealistic. First of all, we assumed that the frictional force was independent of velocity; i.e. no viscous friction. While this assumption is often used when modeling friction; viscous friction most certainly exists in small amounts in our bearing lubrication. Similarly, we assumed that the frictional force was independent of chain tension, which itself is a function of the input force.

The only real way to mitigate all these assumptions would be to measure the efficiency of bike while someone is riding it. While possible, this method makes the input and output forces substantially harder to measure, and we were unable to find a good way to measure efficiency in this manner without significant time investment. However, we did try to make the input force as close to 75N as our experimental setup permitted.

This study, however, was not meant to quantitatively measure the efficiency of our bikes, but instead, to comparatively measure the efficiency of our two bikes. Regardless of how accurate our method was, we used the same method on both bikes, and our source of error on both bikes is the same. In this regard, the study was successful in mitigating our fears that a rear-wheel drive bike would be less efficient than our previous bikes, and therefore effectively informed our design decision.

4.2 SPEED AND STABILITY TESTING

The objective of the speed and stability comparison testing was to determine how the design of the 2009 vehicle affected its performance, as compared to previous Olin competition vehicle designs. We were unsure to how much the major changes to the vehicle, such as rear wheel drive and a higher seating position, would affect speed versus stability performance. After short test rides, riders felt that the prototype vehicle design was more stable and easier to ride, but were unsure about its speed capabilities. In order to quantify the difference, comparative tests were completed. The 2007-08 vehicle, *Vega*, and the 2008-09 prototype vehicle were put through a series of identical test courses.

In order to test the stability and handling of each vehicle, a slalom course was set up in a parking lot. Seven cones, ten feet apart were placed in a line. A male and a female rider would each have three chances to maneuver through the cones on each vehicle, as shown in Figure 17. The number of cones successfully completed after each trial was recorded. Before each set of three trials, the rider had a few minutes to familiarize themselves with each vehicle.



FIGURE 17: THE FEMALE RIDER MANEUVERING THROUGH THE CONES ON THE VEGA FOR THE STABILITY AND HANDLING TEST.

After completing the tests, speaking with the riders, and analyzing the data, it was clear that the prototype is more stable and has greater handling than the *Vega* design. The completed cone data for each rider can be seen in Table 10.

| Vehicle | Rider | Trial 1 | Trial 2 | Trail 3 | Average |
|-----------|--------|---------|---------|---------|------------|
| Vega | Male | 0 | 1 | 2 | 1 |
| | Female | 2 | 4 | 3 | 3 |
| Prototype | Male | 6 | 7 | 7 | 6.7 |
| | Female | 7 | 5 | 7 | 6.3 |

TABLE 10: STABILITY AND HANDLING RESULTS (NUMBER OF COMPLETED CONES) FOR BOTH MALE AND FEMALE RIDERS.

Though the speed of each trial was not measured, observers noted that the riders were able to maneuver the cones much more quickly and confidently in the prototype vehicle than in the *Vega*. The riders much preferred the prototype to the previous design as well.

Quantifying the performance of the prototype vehicle against the previous vehicle design of the *Vega* allowed the team to make informed design decisions before finalizing the design for *Helios*. The frame geometry, higher seating position and shorter wheel base, of the prototype were kept relatively the same for the competition vehicle. It is believed that the increased stability and handling will also increase rider confidence, which will also contribute positively to competition performance.

4.3 FAIRING CONSTRUCTION TESTING

To validate our innovative fairing construction concept and prove that all our MATLAB code was calculating and plotting the correct shapes for the ribs (elliptical shapes perpendicular to long axis) and spars (lengthwise members) of our fairing, we needed to some scale models. The plotted ribs and spars were scaled to produce a small model about 8in long, printed, and cut directly from the printed paper sheets. It became obvious immediately that we needed some way to identify each rib and spar on the printed sheet. After some trial and error, the model was assembled (shown in Figure 18), with many lessons learned. Based on the experience with this model, a set of instructions was written to lay out proper assembly, and the program was modified to plot an identifying mark on each rib and spar so they could be assembled without difficulty.

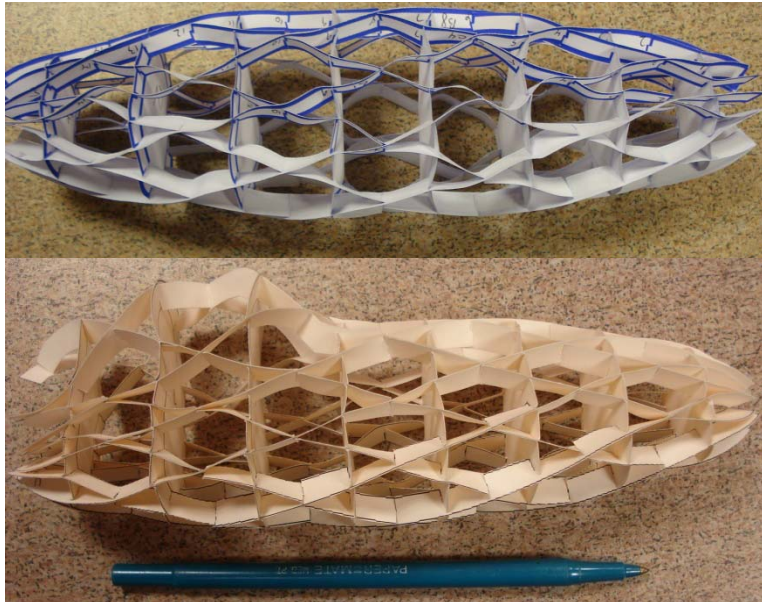


FIGURE 18: (TOP) OUR INITIAL FAIRING SCALE MODEL. NOTE WAVINESS IN SPARS DUE TO THIN PAPER CONSTRUCTION. (BOTTOM) SECOND SCALE MODEL, SHOWING DENSITY ISSUE AROUND CANOPY.

The paper used for the first model presented many problems in assembly, so we transferred the plotted ribs and spars to cardboard for a second attempt (shown in Figure 18). For this second model we also used a fairing shape with a canopy, a more complex shape that would really test our program. The most apparent problem with this second model was the density of the lattice around the canopy. The complex shape necessitates a more densely packing of ribs and spars to define it well than the simple ellipsoid shape. We have devised several solutions for this issue and will probably end up simply doubling the density of ribs and spars output by the program and then only using the additional ribs and spars in the regions which need more definition, such as the canopy and nose of the fairing. We are currently in the middle of building a third scale model using the fairing shape chosen by our analysis, and beginning assembly on a full scale assembly of the ribs and spars.

4.4 ROLL BAR TESTING

To meet competition safety rules, we had to prove that our roll bar could withstand 600lbs of load at 12° from the vertical, and 300lbs of side load. Because we do not have a large tensile testing machine on campus, we performed this test in the Olin College weight room by tilting the bike backward by 12° and hanging free weights off the roll bar. As consistent with our FEA, the roll bar did not plastically or elastically deform by more than 2in. Figure 19 shows our successful test; the two people touching the bike are only applying a horizontal force to keep the bike from tipping.



FIGURE 19: LEFT IS THE ROLL BAR SUCCESSFULLY WITHSTANDING 600LB LOAD AT 12° FROM VERTICAL. RIGHT SHOWS ROLL BAR UNDER 300LB SIDE LOAD. TEAM MEMBERS STANDING ON REAR FORK AND SEATED IN FOREGROUND ARE PROVIDING REACTION FORCES TO COUNTER THE MOMENT APPLIED BY THE LOAD.

We performed a similar side-loading test on the roll bar. We mounted the bike in the same fashion but looped the loading rope over a pulley to apply a side load on the bike, as shown in Figure 19. Again, as predicted by our FEA, the roll bar did not fail the 300lb side-load test.

5 SAFETY

Roll Bar: The roll bar has been field tested on the vehicle since December. It has passed both loading tests without deforming into the rider and entirely encompasses the widest part of the rider from both top and sides.

Seat Belt: Our seat belt is an automotive-quality four point harness that is structurally attached to vehicle.

Steering System: The steering system consists of two parallel tie rods with an adjustable handle position to accommodate our range of rider sizes. This system is similar to our previous steering mechanisms and has been successfully field tested on the prototype. The steering is specifically designed to not jiggle or otherwise impinge on the rider's ability to control the vehicle.

Sharp Edges: We have not discovered any sharp edges on *Helios*; however, if we find any dangerous edges, we have the capability to remove them.

Open Tube Ends: The current version of the bicycle has no open tube ends except for the center of the back fork. The tube end, however, is less than a one inch long, difficult to access, and both deburred and painted. It is also part of the back fork, so was successfully incorporated on a previous bicycle.

Pinch Points: Our bicycle has a couple of pinch points. The front chain runs between the rider's legs for a short distance before dropping lower. However, this interference occurs well away from the thickest part of the rider's legs. Also, the seat clamps could pinch someone when adjusting the seat. For this reason, we do not grip the bike by the bottom tube.

Other Hazards: The bicycle has no other obvious hazards.

Field of View: Currently, we have not yet fabricated the fairing. However, our fairing design includes a large wrapping plexiglass window that provides extensive front and side visibility.

Design for Safety: We have included several additional safety precautions for the bicycle.

- 1) *Fairing Material:* Our fairing design includes extra Kevlar plies on the portions of the fairing most likely to hit the ground, acting as extra rider protection in addition to the roll bar.
- 2) *Frame Support:* Our seat clamp design requires the addition of a second tube below the horizontal member. This tube keeps the seat from rotating, but also acts as an extra supporting member below the rider.
- 3) *Clipless Pedals:* If the bike tips, the rider's legs are constrained by the pedals and therefore do not leave the protection of the roll bar.
- 4) *Elbow Pads:* Similar to last year, our riders will be wearing elbow pads during the event as extra precaution against roadburn.

6 BIBLIOGRAPHY

American Bamboo Society. 2008. Bamboo Bicycle. [Online] October 26, 2008. [Cited: November 10, 2008.] <http://www.americanbamboo.org/GeneralInfoPages/BambooBicycle.html>.

Brown, Sheldon, et al. Harris Cyclery Articles. [Online] [Cited: March 9, 2009.] <http://sheldonbrown.com/articles.html>.

Carroll, Douglas R. 2003. *The Winning Solar Car*. Warrendale PA : SAE International, 2003.

Sheldrake. 2009. Cardboard Surfboards. [Online] March 2009. [Cited: November 20, 2008.] <http://www.sheldrake.net/cardboards/>.

Smith, Carroll. 1985. *Engineer to Win*. Osceola WI : Motor Books, 1985.

Vandermark, Rob. 2009. *Tour of Seven Cycles*. Watertown MA, January 26, 2009.

Wikipedia. Density of Air. [Online] [Cited: March 12, 2009.] http://en.wikipedia.org/wiki/Density_of_air.

—. Drag Equation. [Online] [Cited: March 12, 2009.] http://en.wikipedia.org/wiki/Drag_equation.

Wilson, David Gordon. 2004. *Bicycling Science*. Cambridge : The MIT Press, 2004.

Wired.com. 2008. Bamboo Bike Maker Grows His Frames, Bonsai Style. *Gadget Lab*. [Online] September 25, 2008. [Cited: November 10, 2009.] <http://blog.wired.com/gadgets/2008/09/growing-bamboo.html>.

**Rules for the
2009 Human Powered Vehicle Challenge East
Sponsored by ASME and Drexel University**

**Appendix 5: Vehicle Description
Due March 20, 2009**

(Dimensions in inches, pounds)

Competition Location: Philadelphia, PA

School name: Olin College

Vehicle name: Helios

Vehicle number 5

Vehicle type Single X Multi-rider Utility

Vehicle configuration

Upright Semi-recumbent X

Prone Other (specify)

Frame material 4130 Chro-moly tubing

Fairing material(s) Fiberglass and Kevlar, cardboard honeycomb

Number of wheels 2

Vehicle Dimensions

Length 78 Width 24

Height 48 Wheelbase 52

Weight Distribution Front 20 Rear 20 Total 40

Wheel Size Front 16 Rear 20

Frontal area

Steering Front X Rear

Braking Front X Rear Both

Estimated Cd 49.29 in² (this is CdA, we don't have them separate)

Vehicle history (e.g., has it competed before? where? when?)

Never been to competition
